physical sciences forum

MDPI

Proceeding Paper

Photoemission Spectra from Al(111) Surface: Jellium and Band-Structure-Based Potentials †

Martín Barlari [1,2,*], Renata Della Picca [3], Darío M. Mitnik [1] and Diego G. Arbó [1,2,4,*]

[1] Instituto de Astronomía y Física del Espacio—IAFE (CONICET-UBA), Buenos Aires 1428, Argentina; dario@iafe.uba.ar
[2] Departamento de Física, Facultad de Ciencias Exactas y Naturales, Universidad de Buenos Aires, Buenos Aires 1428, Argentina
[3] Instituto Balseiro (UNCuyo), Centro Atómico Bariloche (CNEA) and CONICET, Bariloche 8400, Argentina; renata@cab.cnea.gov.ar
[4] Ciclo Básico Común, Universidad de Buenos Aires, Buenos Aires 1428, Argentina
* Correspondence: mbarlari@iafe.uba.ar (M.B.); diego@iafe.uba.ar (D.G.A.)
† Presented at the 1st International Online Conference on Atoms, 29–30 January 2026; Available online: https://sciforum.net/event/IOCAT2026.

Abstract

We theoretically compare the photoemission spectra of an Al(111) surface under a short laser pulse using two unidimensional models: jellium and band-structure-based (BSB). We solve the time-dependent Schrödinger equation and project the propagated wave-function onto scattering states via the scattering projection method in order to get clean spectra, free of spurious oscillations. The main difference between the jellium and BSB results consists of a displacement of the multiphoton peaks of about 5 eV in energy. We find that there is a combined effect of atomic layers and surface–vacuum interface smoothness on the overall structure of the BSB spectra that explains the energy shift in the first multiphoton peak. We also present an energy-band analysis of the photoionization spectra that accounts for their structure within the two surface models.

Keywords: photoionization; surfaces; attophysics; aluminum; band-structure-based; scattering projection method

1. Introduction

Photoionization of solids has been an open area of research in recent decades [1–3]. In cases such as electron emission from solid surfaces, the fundamental physics involved can be described using unidimensional models to analyze photoemission from the valence band of metallic surfaces like Al(111), Al(100), Mg(0001) and Be(0001) [4–6]. Two of the most common one-dimensional models for metallic surfaces are the simplistic jellium model [7] and the band-structure-based (BSB) model [6], which incorporates relevant surface properties like corrugation due to atomic layering as well as surface plasmon effects [4,5].

In this work, we focus on photoionization from an Al(111) surface subjected to a short laser pulse. Some differences in the photoionization spectra (PES) employing both models have been reported in previous works, though the origin of this discrepancy has remained an open question until now [4,5,8]. In order to calculate the PES, we must solve the time-dependent Schrödinger equation (TDSE) for the initially bound electron states and then project the final time-propagated wave-function at the end of the laser pulse

Check for updates

Academic Editor: Anand K. Bhatia

Published: 17 July 2026

Copyright: © 2026 by the authors. Licensee MDPI, Basel, Switzerland. This article is an open access article distributed under the terms and conditions of the Creative Commons Attribution (CC BY) license.

onto continuum states. In a recent work [9], we reported that using the standard basis of stationary continuum eigenstates of the unperturbed laser-free Hamiltonian yields large unphysical oscillations in the PES, which are numerical artefacts. We have shown that these spurious oscillations can be avoided by using a continuum basis consisting of scattering states generated by the scattering projection method (SPM) [9]. In particular, the calculations reveal a shift in the energy position of the multiphoton ionization peaks of about 0.2 a.u., which has been suggestively attributed to the rugosity of the BSB potential [9]. To the best of our knowledge, no detailed analysis has been reported regarding this issue.

The goal of this work is to inquire into the differences in the resulting PES from both jellium and BSB potential models. By separately examining the features that distinguish the BSB from the jellium—namely, smoothness, corrugation, and surface state inclusion—we determine their respective influence on the PES, thereby accounting for the observed peak shifts. We find that there is a combined effect of atomic layers and surface smoothness on the overall structure of the BSB spectra that explains the energy shift in the first multiphoton peak. In addition, we perform an energy-band study of the PES that accounts for the structure of both spectra. The effect of the induced surface and bulk fields on photoionization spectra is not considered in this work [5]. We plan to address the topic of this effect on photoionization spectra for different materials in the near future.

The work is organized as follows. In Section 2, the numerical method to compute the PES is described. In Section 3, the results are introduced and discussed. Concluding remarks are presented in Section 4. Atomic units (a.u.) are used otherwise stated.

2. Methods

The focus of this work is the ionization of an Al(111) surface under grazing incident ultrashort laser pulses. The surface is modelled as a one-dimensional short-range potential $V(z)$ where z is the coordinate perpendicular to the material–vacuum interface. The dynamics of the electrons, initially bound to the surface, are described by the TDSE in the single-active electron approach within the dipole approximation:

$$i\frac{\delta}{\delta t}|\psi(t)\rangle = [H_0 + H_{int}(t)]|\psi(t)\rangle. \quad (1)$$

The unperturbed Hamiltonian, $H_0 = p^2/2 + V(z)$, is the sum of the kinetic term and the electron–surface interaction potential energy. The laser pulse perturbation is introduced by the time-dependent external electric field $F(t)$ and it can be read as $H_{int}(t) = z\,F(t)$ in the length gauge, within the dipole approximation.

The simplest possible model for the electron–surface interaction is the jellium model, i.e., $V(z) = -V_0\,\Theta(a/2-|z|)$, in which the active electron is initially bound to a *slab* of width a and depth $V_0 = E_F + \Phi$, where E_F and Φ are the Fermi energy and work function of the material, respectively, and Θ is the Heaviside function. In what follows, we consider an initial electron distribution at zero temperature described by the Fermi statistics.

On the other hand, there is a more realistic BSB model in which the surface is pictured as a collection of atomic planes that together also form a *slab*, accounting for the effects of the band structure of the metal, as the name suggests [6]. The details of the calculation of this potential and the specific parameters used for the Al(111) surface are extracted from Ref. [6]. Here we consider a *slab* consisting of 70 atomic layers surrounded by a vacuum, which corresponds to the asymptotic region of the potential. In order to compare BSB results to jellium results—in both cases modelling Al(111)—we consider a similar jellium model in terms of width and depth to the BSB model. This leads us to define a *slab* width of $a = 312.74$ a.u. and depth $V_0 = 0.57$ a.u. Figure 1a exhibits both basic models considered in this work and we note three key differences between them: (i) smoothing at the interface

between the solid and vacuum regions; (ii) corrugation at the bottom of the BSB potential mimicking the atomic layers, and (iii) a near-to-vacuum oscillation at the bottom, which is responsible for the surface electronic states (SESs). So far, the influence of the three characteristics of the BSB potential on the PES has remained unclear.

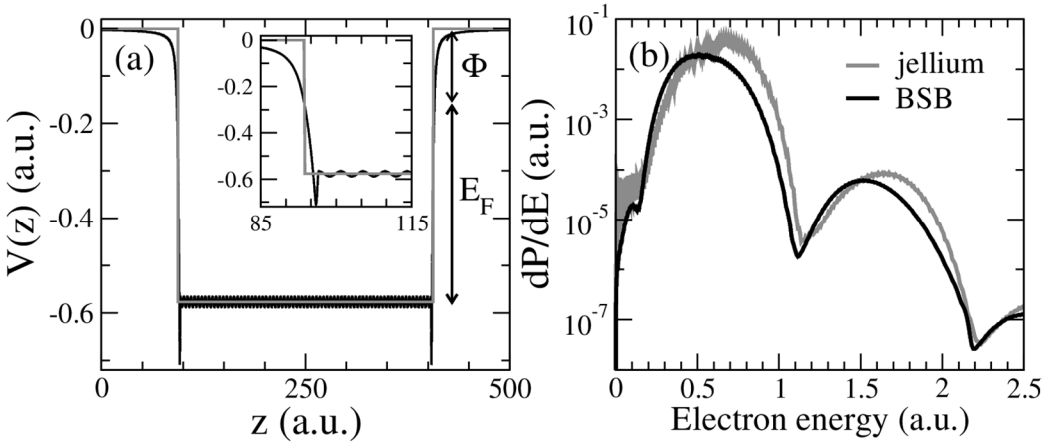


Figure 1. (**a**) Comparison of both surface models, jellium and BSB, with a zoom inset revealing fine details (same axes as main figure). The work function and Fermi energy of the material are $\Phi = 0.156$ a.u. and $E_F = 0.414$ a.u., respectively. (**b**) Photoelectron spectra along the direction perpendicular to the surface of Al(111) using the SPM for the BSB (black line) and jellium (grey line) models. The laser pulse has 6 cycles, peak amplitude $F_0 = 0.1$ a.u., and frequency $\omega = 1$ a.u.

The target surface Al(111) is impinged by an external, grazing incident laser pulse of duration τ, whose time-dependent electric field is given by

$$F(t) = F_0 \, sin^2\left(\frac{\pi t}{\tau}\right) cos(\omega t) \tag{2}$$

for $t \, \epsilon \, (0, \tau)$ and zero elsewhere, where F_0 is the maximum laser amplitude, ω is the main frequency, and $\tau = 2n\pi/\omega$ the pulse duration, comprising n optical cycles. The laser field is also linearly polarized perpendicularly to the surface.

We solve the TDSE in Equation (1) by discretizing the position perpendicular to the surface in a numerical grid of width $L = 500$ a.u. and spacing $\Delta z = 0.2$ and 0.05 a.u. for jellium and BSB, respectively. The values of L and Δz were optimized in order to ensure convergence of the results and to avoid bounces of the wave-function at the edges of the numerical domain (spatial box). Because we guarantee convergence of the numerical calculations and no approximations are done besides the dipole approximation, the results of the TDSE are gauge-invariant. We must also note that the use of periodic boundary conditions is usual in this type of problem [8]. Thus, in the present work we have also investigated the influence of these boundary constraints, finding that the resulting spectra do not vary as long as the space and time grids assure convergence, as expected. That is, there is no variation in the results whether the boundary conditions are "stationary"(zero-valued wave functions at the edges of the box) or "periodic" (same value and derivative at both edges of the box). The corresponding unperturbed Hamiltonian is diagonalized and 108 eigenstates are obtained for the jellium model, of which 92 are initially occupied between the bottom of the potential well at $E = -V_0 = -\Phi - E_F$ and $E = -\Phi$ (see Figure 1a), where the work function is $\Phi = 0.156$ a.u. (4.24 eV) and the Fermi level is $E_F = 0.414$ a.u. (11.26 eV) for Al(111). Executing the same procedure for the BSB potential, we obtain a total of 115 bound eigenstates, of which 91 are initially occupied at energies below the Fermi level, i.e., $E \leq -\Phi$. We compute time propagation of the initial bound states until the end of the laser pulse at $t = \tau$ using the staggered-leapfrog method with

a time step of $\Delta t = 0.00038$ a.u. [10,11]. Then, we project the wave-functions after time propagation onto scattering states with outgoing boundary conditions using the scattering projection method (SPM) introduced recently in Ref. [9]. In that work, we showed that the SPM is more efficient than the widespread window operator method [12,13] in terms of eliminating spurious oscillations and reproducing high-frequency physical oscillations in the energy photoelectron spectra (PES).

In order to construct the total energy-resolved differential photoelectron spectrum dP/dE, we incoherently sum over the projections of all time-evolved wave-functions, one for each initially occupied state [8],

$$\frac{dP}{dE} = 2\sqrt{2E}\,\rho(E)\sum_i \left(\left| \left\langle \Psi_k^{\,l} | \psi_i(\tau) \right\rangle \right|^2 + \left| \langle \Psi_k^{\,r} \,|\, \psi_i(\tau) \rangle \right|^2 \right) \Theta(-E_i - \Phi), \tag{3}$$

where the first factor 2 comes from electron spin degeneracy and $\rho(E)$ is the density of final continuum states of energy $E = k^2/2$ with electron momentum k perpendicular to the surface. By using the Heaviside function $\Theta(-E_i - \Phi)$ we restrict the initial states to those contained below the Fermi level, as commented before. Here, E_i is the initial bound electron energy of the i-th state and $\left\langle \Psi_k^{\,l(r)} \,\middle|\, \psi_i(\tau) \right\rangle$ is the projection of the time-evolved wave-function $\psi_i(\tau)$ of that particular state with the scattering state of momentum k. This last state, $\Psi_k^{\,l(r)}$, is obtained via the SPM [9] and has outgoing boundary conditions describing propagation to the left (right).

3. Results and Discussion

In this section we present the PES for electron emission perpendicular to the Al(111) surface. The laser profile used in all presented calculations has six cycles, $F_0 = 0.1$ a.u. and $\omega = 1$ a.u. We begin by showing, in Figure 1b, the main spectra which trigger the rest of this work, i.e., the comparison of the PES perpendicular to the Al(111) surface using the two baseline models: jellium and BSB. By comparing the spectra in Figure 1b, we find that the photoemission peaks are shifted by about 0.2 a.u. resulting in more energetic maxima for the jellium model. We note that while the BSB model sets the first maximum at an electron energy $E \simeq 0.5$ a.u., the jellium sets it at about 0.7 a.u. Similarly, the second maxima are located approximately at 1.5 and 1.7 a.u. for the respective models. The origin of this shift was attributed to the rugosity of the BSB potential [4,5,8]. However, to our knowledge, no in-depth analysis of this issue has been performed. According to the conservation of energy rule, the peaks of the spectra are expected at positions $N\omega - E_b$, E_b being the average energy of occupied bound states and N the number of photons involved in that peak with frequency ω. For both BSB and jellium models of Al(111), this mean value is $E_b \simeq -0.43$ a.u. Therefore, setting $\omega = 1$ a.u., the peaks are expected to be located at $E_1 \simeq 0.57$ (single-photon ionization), $E_2 \simeq 1.57$ (two-photon ionization), and so on. These are the approximate positions of the peaks in the calculated PES of Figure 1b. Since the FWHM width of the peaks of approximately 0.4 a.u., directly related to the Fermi energy, comprises the mentioned shift, its origin could be related to different energy-weighted averages of the states, which will be tackled later in this work. In addition, there are finer low-energy structures in the PES for both potentials around $E \sim 0.1$ a.u. and oscillations in the jellium PES due to the Ramsauer–Townsend effect which are only reachable by using the SPM continuum basis, as was discussed in [9].

In order to get a better understanding of the specific role played by each of the three characteristics that distinguish the BSB model from the jellium model—smoothness, rugosity, and SES reproducibility, as already outlined above—and to evaluate their influence on the PES, we also constructed three alternative potential models based on the jellium model. Each of these models (see insets of Figure 2) incorporates only one of the three BSB

features, namely, (i) a surface model with a smooth solid–vacuum interface, with the exact smoothness of the BSB model (without rugosity and SESs); (ii) a surface model which only presents the same corrugation at the bottom as the BSB (without smoothness and SESs); and (iii) a jellium model that only has one oscillation at the bottom, responsible for the generation of SESs in the BSB model (without smoothness and corrugation) [4].

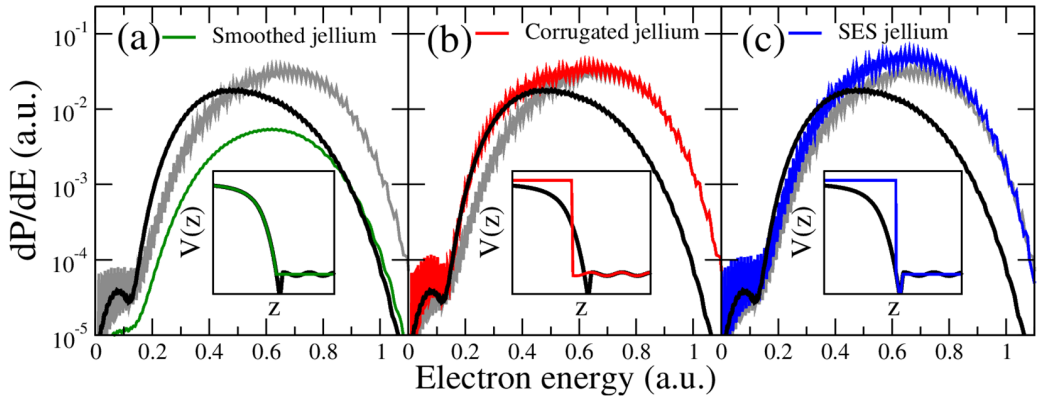


Figure 2. Photoelectron spectra along the direction perpendicular to the surface of Al(111) using the SPM for the BSB (black line) and jellium (grey line) models, subject to the same laser pulse of Figure 1. Comparison with: (**a**) smoothed jellium (green line); (**b**) corrugated jellium (red line) and (**c**) SES jellium (blue line). The insets compare the BSB model with the corresponding modified jellium models.

For the sake of simplicity and relevance, in what follows we focus on the electron energy range corresponding to the first photoionization peak, which has a probability distribution between two and three orders of magnitude higher than the second multiphoton peak (see Figure 1b). In Figure 2, we display the Al(111) PES in this energy range. As before, the black (grey) lines correspond to the BSB (jellium) model, and with coloured lines we have also included the three alternative models described in the previous paragraph.

In Figure 2a, we observe that the ionization probability of the standard jellium model is about two orders of magnitude higher than that achieved using the smoothed jellium model, which indicates a probable strong resonance effect due to the reflections of the wave-packet at the sharp surface edges in the jellium model, whereas in the smoothed jellium model, these reflections disappear, as expected. It is worth noting that the probability distributions of the more energetic part of the peak (falling side) for both the smoothed jellium and BSB models are essentially the same. In this sense, this indicates that the bound energy levels at energies close to the Fermi level are very similar in the smoothed jellium model and the BSB, unlike in the plain jellium model. We also see that softening the walls of the jellium model washes out the Ramsauer–Townsend oscillations present in the plain jellium model, as expected [9], and that this also slightly shifts the main photoionization peaks to lower energies.

The effect of corrugation is evaluated in Figure 2b. There we show that the PES of the corrugated jellium binds the jellium results to the BSB PES at low energies for the peak (rising side). This has a clear explanation from a physical standpoint: corrugation, being located at the bottom of the potential well, primarily affects the lower-energy bound states, increasing their photoionization probability. Instead, in the more energetic falling side of the peak, the corrugated PES sticks to the plain jellium model, which means that the corrugation does not affect the upper-bound states near the Fermi energy level.

The last potential model considered is analyzed in Figure 2c. As can be seen in this graph, the effect of the material layer associated with SESs is very small; that is, the jellium peak is not notoriously displaced. We confirmed this fact by recalculating the BSB spectrum

omitting the SESs as initial states, and we found that the resulting spectrum did not change significantly as compared to the total one with no omissions of initial bound states. A different conclusion is expected for surfaces where the SESs are relevant, as in Al(100) and Be(1000), for example [5]. This will be analyzed in future work.

Finally, in order to understand the partial contribution of the initially bound states of the BSB and jellium models to the PES, we calculate the PES for three sets of initial states (Figure 3). We divide the bound states into three different groups: low-energy bound states ($E_i \lesssim -0.53$), medium-energy bound states ($-0.53 \lesssim E_i \lesssim -0.4$) and high-energy bound states up to the work function of the material ($-0.4 \lesssim E_i \lesssim -\Phi$). The energy ranges are defined such that they all have the same number of states (approximately 30 states per band). In the case of the jellium model (Figure 3a), it is clear that the states that contribute most to the first photoionization peak are those in the high-energy band, with decreasing probability for initially deeper states, where the low-energy band contributes the least. In contrast, for the BSB case (Figure 3b) we observe that the contribution of the three bands is rather similar, with no dominant energy range. On the other hand, in both models the lower-energy band states contribute to the rising side of the photoelectron peak (red curves have their maximums at $E \approx 0.4$ a.u.), the middle-energy band contributes to the middle part of the energy peak (maximums of the green curves are at $E \approx 0.5$ a.u.), and the highest-energy band contributes to the falling side of the photoelectron peak (blue maxima at $E \approx 0.7$ a.u.). As the highest-energy band in jellium has a one-order-of-magnitude greater contribution than the corresponding band in the BSB model, there is a difference in the total energy peak between the two models of about 0.2 a.u., and this explains the peak shift observed in the jellium and BSB models. Furthermore, as the high-energy side of the peak (falling side) is directly related to the softness of the well wall (see Figure 2a and its discussion), the overestimation generated by the jellium states is probably due to the Ramsauer–Townsend resonance due to the multiple bounces at the sharp interface, which are precluded in the BSB model. In conclusion, the jellium model, which clearly has a greater contribution from the states in the highest energy band, has the main photoionization peak shifted towards higher energy. The BSB model does not present that energy shift since it does not have a dominant energy band in its spectra.

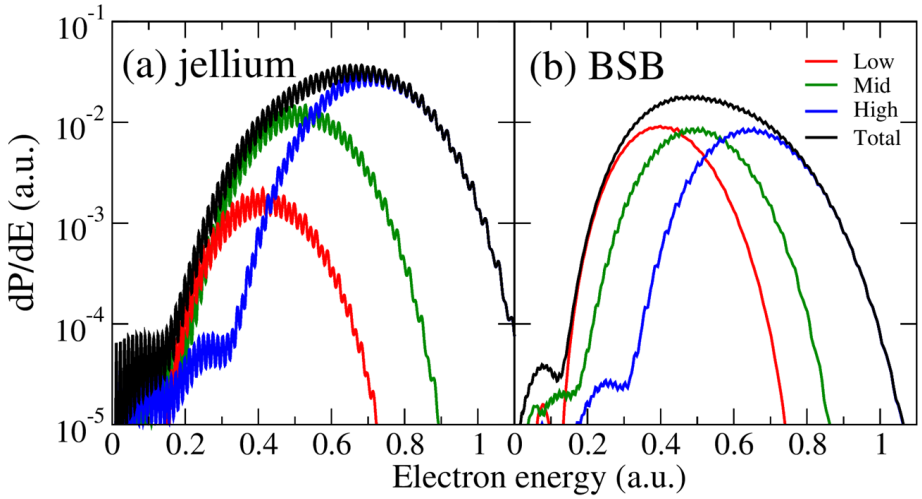


Figure 3. Photoelectron spectra along the direction perpendicular to the surface of Al(111) using the SPM for the (**a**) jellium and (**b**) BSB models, subject to the same laser pulse as in Figure 1. In each case, we show the total spectra (black line), and the spectra restricted to the low- (red line), mid- (green line), and high-energy (blue line) bands.

https://doi.org/10.3390/psf2026013014

4. Conclusions

We have compared the PES of an Al(111) surface using the jellium and BSB potential models by solving the TDSE and projecting the propagated wave-functions onto scattering states via the SPM. This has allowed us to appreciate the main difference in the PES, that consists of a displacement of the multiphoton peaks of about 0.2 a.u. in energy, resulting in more energetic maxima for the jellium model. We have studied the main photoemission peak and found that the origin of this energy shift is attributed to different factors: (i) the smoothing at the edges of the surface potential responsible for the more energetic (falling side) part of the peak; (ii) the corrugation modelling of atomic layers into the solid binds the PES to the BSB at the less energetic rising side of the peak. Contrarily, there is no shift caused by (iii) the material layer associated with SESs. Calculations of the partial PES for different, comparable initial energy-band states show that in the case of the jellium model there is a greater contribution to the first photoionization peak from the high-energy band of the initial states, whereas for the BSB model there is no dominant energy range among the initial states. Summing up, our analysis of the first multiphoton peak explains the origin of the discrepancy in the PES found using the jellium and BSB models and has permitted us to understand the energy shift in terms of a combined effect of the smoothness of the surface–vacuum interface and the corrugation due to the different atomic layers in the bulk modelled in the BSB surface potential, which level the contributing weights of the initial bound states on the PES.

Author Contributions: Conceptualization, D.G.A., M.B. and R.D.P.; methodology, D.G.A., M.B. and R.D.P.; software, M.B. and D.M.M.; validation, M.B.; formal analysis, M.B.; investigation, D.G.A., D.M.M., M.B. and R.D.P.; resources, D.G.A., M.B. and R.D.P.; data curation, M.B.; writing—original draft preparation, D.G.A. and M.B.; writing—review and editing, D.G.A., D.M.M., M.B. and R.D.P.; visualization, M.B.; supervision, D.G.A. and R.D.P.; project administration, D.G.A.; funding acquisition, D.G.A., D.M.M. and R.D.P. All authors have read and agreed to the published version of the manuscript.

Funding: This research was funded by Agencia I+D+i (Argentina), grant numbers PICT 2020-01755 and 2020-01434, and Consejo Nacional de Investigaciones Científicas y Técnicas (CONICET) (Argentina), grant number PIP 2022-2024 11220210100468CO. IPAC—CLEMENTINA XXI, PISCA 142.

Institutional Review Board Statement: Not applicable.

Informed Consent Statement: Not applicable.

Data Availability Statement: The data presented in this study are available upon request from the corresponding author.

Acknowledgments: This work was supported by PICT 2020-01755 and 2020-01434 of ANPCyT (Argentina), and PIP 2022-2024 11220210100468CO of Consejo Nacional de Investigaciones Científicas y Técnicas (CONICET) (Argentina).

Conflicts of Interest: The authors declare no conflicts of interest.

Abbreviations

The following abbreviations are used in this manuscript:

TDSE	Time-dependent Schrödinger equation
PES	Photoelectron spectrum
SPM	Scattering projection method
BSB	Band-structure-based
SES	Surface electronic state
FWHM	Full width at half maximum

References

1. Cavalieri, A.L.; Müller, N.; Uphues, T.; Yakovlev, V.S.; Baltuška, A.; Horvath, B.; Schmidt, B.; Blümel, L.; Holzwarth, R.; Hendel, S.; et al. Attosecond spectroscopy in condensed matter. *Nature* **2007**, *449*, 1029–1032. [CrossRef] [PubMed]
2. Neppl, S.; Ernstorfer, R.; Bothschafter, E.M.; Cavalieri, A.L.; Menzel, D.; Barth, J.V.; Krausz, F.; Kienberger, R.; Feulner, P. Attosecond time-resolved photoemission from core and valence states of magnesium. *Phys. Rev. Lett.* **2012**, *109*, 087401. [CrossRef] [PubMed]
3. Ossiander, M.; Riemensberger, J.; Neppl, S.; Mittermair, M.; Schäffer, M.; Duensing, A.; Wagner, M.S.; Heider, R.; Wurzer, M.; Gerl, M.; et al. Absolute timing of the photoelectric effect. *Nature* **2018**, *561*, 374–777. [CrossRef] [PubMed]
4. Ríos Rubiano, C.A.; Gravielle, M.S.; Mitnik, D.M.; Silkin, V.M. Band-structure effects in photoelectron-emission spectra from metal surfaces. *Phys. Rev. A* **2012**, *85*, 043422. [CrossRef]
5. Ríos Rubiano, C.A.; Della Picca, R.; Mitnik, D.M.; Silkin, V.M.; Gravielle, M.S. Induced-field enhancement of band-structure effects in photoelectron spectra from Al surfaces by ultrashort laser pulses. *Phys. Rev. A* **2017**, *95*, 033401. [CrossRef]
6. Chulkov, E.V.; Silkin, V.M.; Echenique, P.M. Image potential states on metal surfaces: Binding energies and wave functions. *Surf. Sci.* **1999**, *437*, 330–352. [CrossRef]
7. Faraggi, M.N.; Gravielle, M.S.; Mitnik, D.M. Interaction of ultrashort laser pulses with metal surfaces: Impulsive jellium-Volkov approximation versus the solution of the time-dependent Schrödinger equation. *Phys. Rev. A* **2007**, *76*, 012903. [CrossRef]
8. Ríos Rubiano, C.A. Interacción Dinámica Rápida de Partículas y Campos Electromagnéticos con Superficies Metálicas. Ph.D. Thesis, Universidad de Buenos Aires-CONICET. Instituto de Astronomía y Física del Espacio (IAFE), Buenos Aires, Argentina, 2015. Available online: https://bibliotecadigital.exactas.uba.ar/collection/tesis/document/tesis_n5685_RiosRubiano (accessed on 1 July 2025).
9. Barlari, M.; Arbó, D.G.; Gravielle, M.S.; Mitnik, D.M. Elimination of spurious oscillations on photoemission spectra. *Eur. Phys. J. D* **2025**, *79*, 93. [CrossRef]
10. Moler, C.; van Loan, C. Nineteen Dubious Ways to Compute the Exponential of a Matrix. Twenty-Five Years Later. *SIAM Rev.* **2003**, *45*, 3–49. [CrossRef]
11. Press, W.H.; Teukolsky, S.A.; Vetterling, W.T.; Flannery, B.P. *Numerical Recipes 3rd Edition: The Art of Scientific Computing*, 3rd ed.; Cambridge University Press: Cambridge, UK, 2007.
12. Schafer, K.J.; Kulander, K.C. Energy analysis of time-dependent wave functions: Application to above-threshold ionization. *Phys. Rev. A* **1990**, *42*, 5794–5797. [CrossRef] [PubMed]
13. Schafer, K.J. The energy analysis of time-dependent numerical wave functions. *Comput. Phys. Commun.* **1991**, *63*, 427–434. [CrossRef]

Disclaimer/Publisher's Note: The statements, opinions and data contained in all publications are solely those of the individual author(s) and contributor(s) and not of MDPI and/or the editor(s). MDPI and/or the editor(s) disclaim responsibility for any injury to people or property resulting from any ideas, methods, instructions or products referred to in the content.